reported that TGF-β1 expression is mostly observed in the endothelial cells of the vessels in the LF, and not in the fibroblasts of the LF. They also showed that the expression of TGF-β1 mRNA shows a negative linear correlation with the LF thickness, and concluded that not only TGF-β1 but also other cytokines or growth factors play important roles in the process of the hypertrophic changes.

Bone morphogenetic proteins (BMPs) are the largest subgroup in the TGF-β superfamily, and play important roles during embryogenesis and chondrogenesis. BMPs regulate many processes including cellular proliferation, differentiation, extracellular matrix synthesis, and cell survival in various cell types.[10–14] BMPs also have important roles in chondrogenic differentiation. Several studies have reported that TGF-β1 and BMPs synergistically induce chondrogenesis and cartilage matrix production in mesenchymal stem cells and fibroblasts in vitro.[12,15] BMPs also play important roles in several physiological and pathologic conditions of the spine such as ossification of spinal ligaments, intervertebral disc degeneration, and fracture repair.[16–19] However, there have been a few studies about the expressions of BMP signaling components in the hypertrophied LF.

The aims of these histopathological investigations were (1) to clarify the effects of hypermobility and their relationships with the histological features of the hypertrophied LF, (2) to investigate the difference in cellularity between the control LF of the patients with lumbar disc herniation (LDH) and hypertrophied LF of the patients with DLCS, and (3) to confirm the expressions of BMP signaling components in the hypertrophied and control LF.

MATERIALS AND METHODS

A total of 133 LF specimens were obtained from 125 patients who underwent lumbar spinal surgery for symptomatic DLCS. There were 61 male and 64 female patients, with a mean age at surgery of 67.8 years (range, 49 to 85 y). Their diagnoses were made based on their symptoms and radiographic findings. Patients with previous lumbar spine surgery, pyogenic spondylitis, and ossification of the LF were excluded from the study. The LF tissues were carefully harvested en bloc from one side after detachment from the lamina and facet joints.

As controls, 17 LF specimens were obtained from 17 patients with LDH at the time of surgery. The controls consisted of 4 women and 13 men with a mean age at surgery of 52.5 years (range, 32 to 83 y).

The study protocol was approved by the Institutional Review Board of our institution (Approval number: 1603).

Radiographic Evaluation

The thickness of the LF in each patient was measured on an axial T1-weighted magnetic resonance image at the facet joint of the affected spinal level using the Scion Image software (Scion Corporation, Frederick, MD; downloaded from www.microsoft.com/DirectX/).[6] The measurement was repeated at least 3 times and the average of the 3 measurements was recorded as the final thickness of the LF.

To analyze the influence of mechanical stress, the DLCS specimens were divided into 2 groups with hypermobility and without hypermobility. Lumbar spinal hypermobility was diagnosed on the basis of findings in dynamic lateral lumbar radiography. The radiographic measurements were taken using earlier described methods (Table 1).[20] Positive hypermobility was defined when the sagittal disc angulations in the affected level were −5 degrees in the flexion position or greater than 10 degrees in the extension position and/or when the sagittal translation was greater than 3 mm from the neutral to the flexion position.[21]

TABLE 1. Demographic Data of the Patients

Variable	Control (n = 17)	DLCS Without Hypermobility (n = 64)	DLCS With Hypermobility (n = 61)
Mean age in years (range)	52.5 ± 14.8 (32-83)	67.8 ± 8.4* (47-82)	67.7 ± 9.3* (49-85)
Sex			
Male	13	31	30
Female	4	33	31
Level of harvested LF (n)			
L1/2	3	0	0
L2/3	3	7	2
L3/4	0	31	10
L4/5	6	27	45
L5/6	2	2	5
L5/S	3	1	3
Total	17	68	65
Mean thickness of LF (mm)	2.39 ± 0.45	5.08 ± 0.87*	5.43 ± 0.99*
Mean sagittal disc angulation (degree)			
Flexion	−0.4 ± 2.9	−0.7 ± 2.3	−3.4 ± 4.6
Extension	7.0 ± 2.1	7.6 ± 2.5	7.8 ± 4.9
Sagittal translation (mm)	0.9 ± 0.8	1.1 ± 1.0	7.1 ± 3.8

*$P < 0.0001$ when compared with control group.
DLCS indicates degenerative lumbar canal stenosis; LF, ligamentum flavum; n, number of patients.

Histological Examination

The dural layer of the interlaminar portion of the LF was examined after removing excess connective tissue. Each LF specimen was fixed in 10% neutral-buffered formalin, decalcified with 10% ethylene diaminetetraacetic acid for 48 hours, cut sagittally and embedded in paraffin blocks. Thin slices of 4 μm were obtained and were subjected to the following staining methods: elastica van Gieson (EVG) staining to examine the condition of elastic fibers; hematoxylin and eosin (H&E) staining to evaluate the cellular distribution; and toluidine blue (TB) staining to evaluate the cartilage matrix restoration area.

Immunohistochemistry

Immunohistochemistry was performed using the avidin-biotin-peroxidase complex method for single staining. Sections (4 μm thick) were deparaffinized and were treated with proteinase K (6 μg/mL) for 30 minutes for antigen retrieval. The endogenous peroxidase activity was blocked by incubation in methanol containing 0.3% H_2O_2 for 10 minutes. After blocking with 2% bovine serum albumin solution containing 0.1% Triton X-100 for 1 hour, the sections were incubated at 4°C overnight with one of the following primary antibodies: mouse monoclonal antitype 2 collagen (Daiichi Fine Chemicals, Tokyo, Japan; optimum dilution, 1:50); goat polyclonal anti-BMP receptor (BMPR)-1A, anti-BMPR-1B, anti-BMPR-2, anti-BMP-2, and anti-BMP-7 (Santa Cruz Biotechnology, Santa Cruz, CA; optimum dilution, 1:50); mouse monoclonal anti-BMP-4 (Chemicon International, Temecula, CA; optimum dilution, 1:50); and rabbit polyclonal antiphospho-Smad1/5/8 (Cell Signaling Technology, Beverly, MA; optimum dilution, 1:200). On the next day, the sections were incubated with appropriate biotinylated secondary antibodies (Vector Laboratories Inc., Burlingame, CA) for 1 hour. The avidin-biotin-peroxidase complex (Vectastain ABC Kit; Vector Laboratories Inc) was then added for 1 hour, and the color reaction was developed using 3,3′-diaminobenzidine tetrachloride (Sigma Chemical Co., St Louis, MO) diluted in 0.05 M *Tris*-HCl (pH 7.6) containing phosphate-buffered saline and 0.3% H_2O_2 for 5 minutes. Nuclear counterstaining was carried out with hematoxylin.

To identify the characteristics of the cells expressing BMPRs, immunofluorescence staining was performed with the following primary antibodies: monoclonal mouse anti-CD105 (Santa Cruz Biotechnology; optimum dilution, 1:50) as a marker of mesenchymal stem cells or vascular endothelial cells; polyclonal rabbit anti-Msx2 (Santa Cruz Biotechnology; optimum dilution, 1:50) as a marker of mesenchymal stem cells or undifferentiated cells; and polyclonal rabbit anti-Sox9 (Santa Cruz Biotechnology; optimum dilution, 1:50) as a marker of chondrocytes. Different colors of fluorescent-tagged donkey antigoat or antirabbit antibodies conjugated to Alexa Fluor 488, 594, and 688 (Invitrogen, Carlsbad, CA) were used as secondary antibodies. Nuclear counterstaining was carried out with Hoechst 33258.

Quantification

Histologically and immunohistochemically stained sections were evaluated using a light microscope (Model BX50; Olympus Optical Co., Ltd, Tokyo, Japan). In H&E staining, the numbers of cells were counted in 5 random fields (442 × 332 μm, total of 0.73372 mm^2 for the 5 random fields at × 40 magnification) in the center of LF tissue images captured digitally using an RT Slider Spot Digital Camera (Model DP70; Olympus Optical Co., Ltd). The percentages of elastic fiber areas stained black using the EVG method were analyzed using the Scion Image software. For analyses of the cartilage matrix area after TB staining, 5 random fields in the center of LF sections were captured digitally and the percentages of the metachromatic areas were measured using the Scion Image software and the threshold technique. Data are presented as mean ± SD.

Statistical Analysis

The Bonferroni method was used for comparison among 3 groups. The relationship between 2 values was determined by the Pearson correlation test. P values of less than 0.05 were considered to be statistically significant.

RESULTS

Histological Findings

EVG staining showed a loss of elastic fibers with fragmentation and an irregular arrangement accompanied by an increase in collagen fibers in the degenerated LF (Fig. 1). In the control group, the LF was rich in elastic fibers in a regular pattern with a small number of collagen fibers among the elastic fibers. The percentages of elastic fibers per area were significantly lower in the DLCS with and without hypermobility groups than in the control group. There were no significant differences between the DLCS with and without hypermobility groups (Table 2).

H&E staining showed that the number of cells was increased in the hypertrophied LF, especially in the densities of hypertrophic chondrocytes, which have a large cytoplasm and a perinuclear clear zone, and that immature chondrocytes, which have a small cytoplasm with a small round nuclear zone, were remarkably increased (Fig. 1). In contrast, there were a few chondrocytes in the control LF. The cellularity was significantly higher in the DLCS with hypermobility group than in the DLCS without hypermobility group (132.1 ± 52.1 vs 97.7 ± 34.8 cells/mm^2; $P < 0.0001$) and the control group (132.1 ± 52.1 vs. 34.6 ± 39.5 cells/mm^2; $P < 0.0001$) (Table 2). The cellularity showed a positive and significant correlation with the LF thickness in magnetic resonance image ($r = 0.46$; $P < 0.0001$) (Fig. 2A).

TB staining showed that red-purple areas, which are known to represent metachromasia indicating cartilage-specific matrix, were prominently increased in the degenerated LF accompanied by numerous proliferating cells (Fig. 1). These cells and the matrix in their vicinity

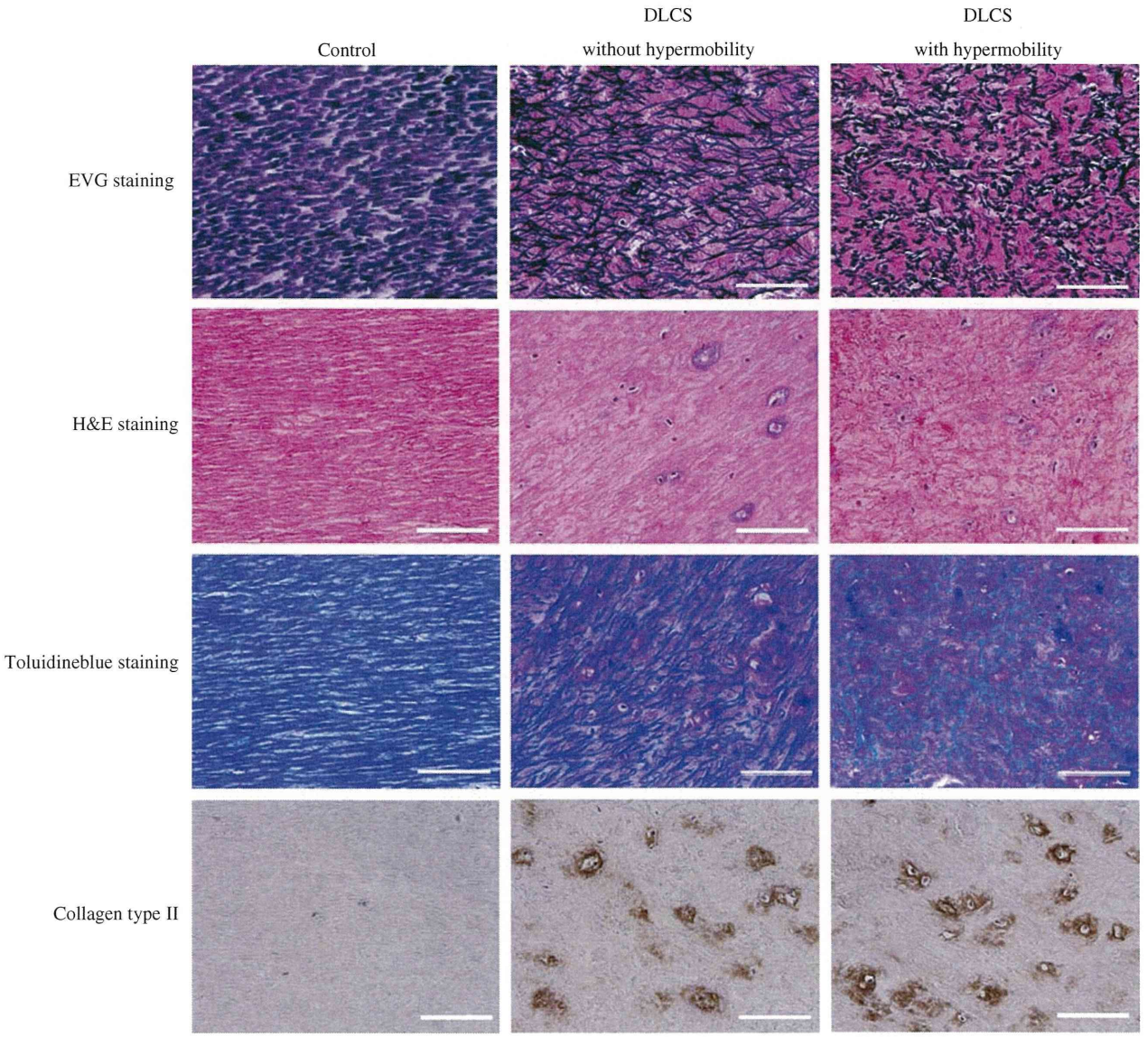

FIGURE 1. Histological findings after elastica van Gieson (EVG), hematoxylin and eosin (H&E), and toluidine blue staining, and immunohistochemistry as well, for collagen type 2 (×400; scale bars = 100 μm). The elastic fibers are rich and show a regular arrangement in the control group, whereas they are decreased and show an irregular pattern or fragmentation in the degenerative lumbar canal stenosis (DLCS) groups (top row). The cell number is increased in the DLCS groups compared with the control group (second row). The cartilage matrix area is small in the control group, but is increased in the DLCS groups, especially in the DLCS with hypermobility group (third row). Collagen type 2 shows positive staining in the ligamentum flavum of the DLCS with and without hypermobility groups but is not stained in the control group (fourth row).

were positively stained with an antitype 2 collagen antibody by immunohistochemistry (Fig. 1). The percentage of the cartilage matrix area was significantly higher in the DLCS with hypermobility group than in the DLCS without hypermobility group (62.0 ± 27.7% vs 35.7 ± 25.0%; $P < 0.0001$) and the control group (62.0 ± 27.7% vs 9.2 ± 12.7%; $P < 0.0001$) (Table 2). There was also a positive and significant correlation between the percentage of the cartilage matrix area and the LF thickness ($r = 0.41$; $P < 0.0001$) (Fig. 2B).

Immunohistochemical Findings

Expressions of all 3 BMPR types (BMPR-1A, BMPR-1B, and BMPR-2) were observed not only in chondrocytes near the enthesis, but also in hypertrophic chondrocytes, fibroblast-like spindle cells, and immature chondrocytes in the central portion of the hypertrophied LF tissue (Fig. 3). The percentage of immunopositive cells for each BMPR type was significantly higher in the DLCS with hypermobility group than in the DLCS without hypermobility group ($P < 0.0001$) and the control group

TABLE 2. Quantification of Histopathological Staining

	Control	DLCS Without Hypermobility	DLCS With Hypermobility
% elastic fiber	57.1 ± 17.4	40.2 ± 7.2*	38.6 ± 9*
% cartilage matrix	9.2 ± 12.7	35.7 ± 25.0*	62.0 ± 27.7*,†
Cellularity	34.6 ± 39.5	97.7 ± 34.8*	132.1 ± 52.1*,†

% elastic fiber: the percentage of elastic fiber area in total area.
% cartilage matrix: the percentage of cartilage matrix area in total area cellularity; cell number per mm^2.
*$P < 0.0001$ when compared with control group.
†$P < 0.0001$ when compared with DLCS with and without hypermobility groups.
DLCS indicates degenerative lumbar canal stenosis.

($P < 0.0001$) (Fig. 4). Expressions of BMP-2, BMP-4, and BMP-7 were mainly observed in chondrocytes, with a few positively stained fibroblast-like spindle cells (Fig. 5). Expression of phospho-Smad1/5/8 was detected in many cells and the distribution of these immunopositive cells was similar to that of the BMPR-immunopositive cells (Fig. 5). These results suggest that the BMP signaling pathway is activated in hypertrophied LF specimens. In the control specimens, BMPs and BMPRs were weakly expressed in the enthesis in which the ligament connected to the bone but neither BMPs nor their receptors were expressed in the center portion of the specimens (Figs. 4, 5).

To confirm which cell types expressed BMPRs, we performed double or triple fluorescence staining with Msx2, CD105, and Sox9. Some cells positive for BMPR-1A, BMPR-1B, and BMPR-2 also expressed Sox9 or both

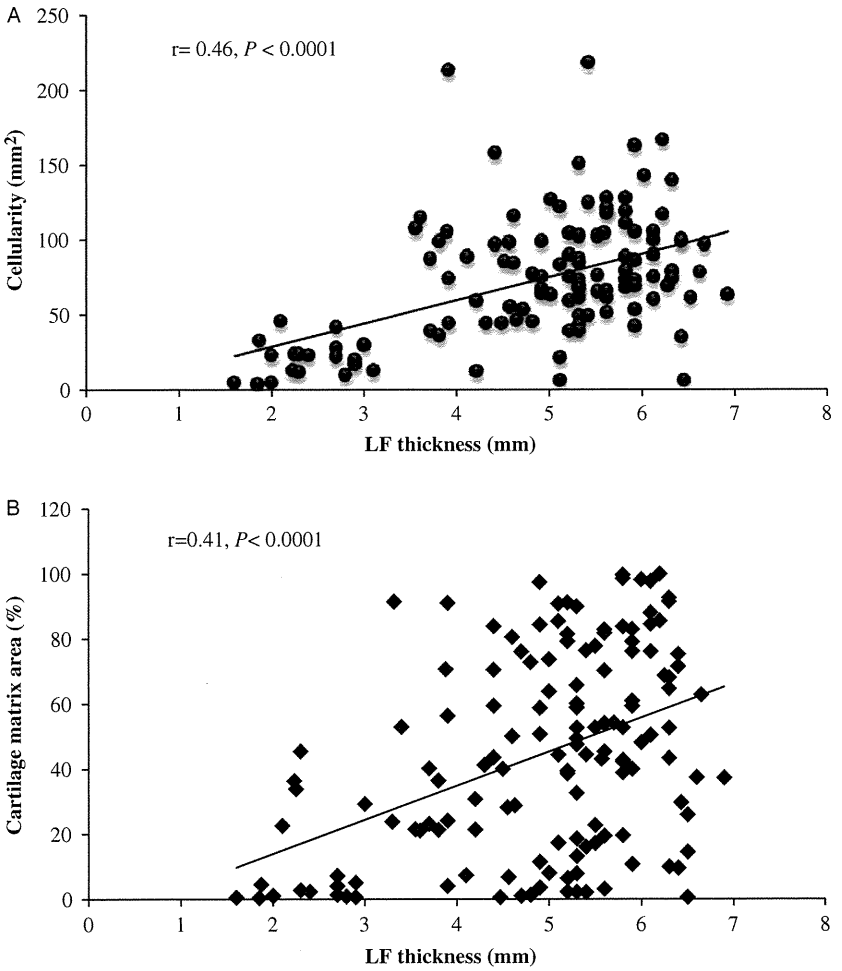

FIGURE 2. A, Relationship between the ligamentum flavum (LF) thickness and the cellularity. The cellularity shows a positive correlation with the LF thickness ($r = 0.46$; $P < 0.0001$). B, Relationship between the LF thickness and the percentage of the cartilage matrix area. The percentage of the cartilage matrix area shows a positive correlation with the LF thickness ($r = 0.41$; $P < 0.0001$).

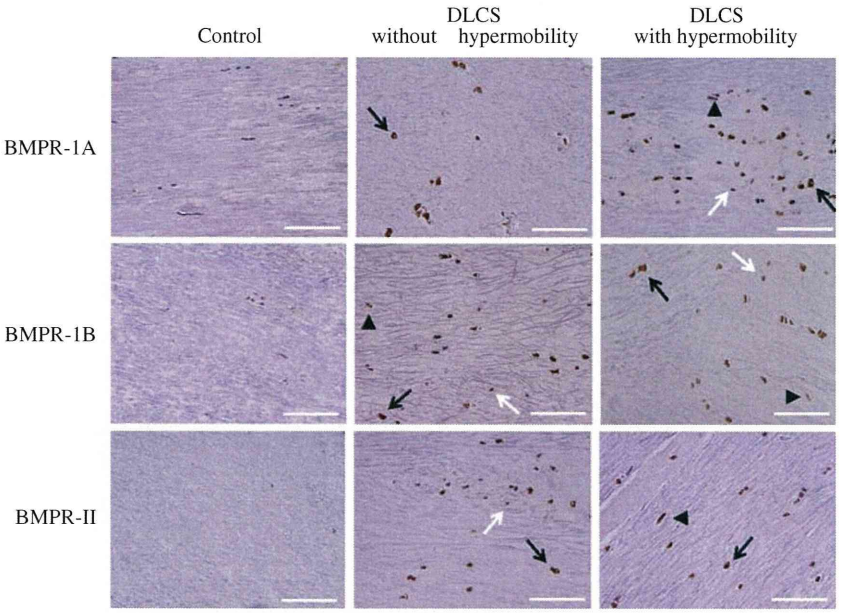

FIGURE 3. Immunohistochemical findings for BMPR-1A, BMPR-1B, and BMPR-2 (×400; scale bars = 100 μm). The immunoreactivity for each BMPR is much stronger in the DLCS with hypermobility (right column) and without hypermobility groups (middle column) than in the control group (left column). Black arrows: hypertrophic chondrocytes; white arrows: immature chondrocytes; black arrowheads: fibroblast-like spindle cells. BMPR indicates bone morphogenetic protein receptors; DLCS, degenerative lumbar canal stenosis.

CD105 and Msx2 in the degenerated LF (Fig. 6). However, no coexpression was seen in the control specimens (data not shown).

DISCUSSION

The histological findings obtained in this study showed that the cellularity was significantly increased in the degenerative LF and had a positive correlation with the LF thickness. Most of these cells were positive for collagen type 2, and therefore were identified as chondrocytes. In the DLCS groups, these chondrocytes were observed even in the center of the LF, whereas chondrocytes only existed in the enthesis in which the ligament was attached to the bone in the control group. Yoshida et al[5] reported that proliferation of chondrocytes was observed in 91% of patients with DLCS, which is consistent with our observations. In this study, we quantified the cartilage matrix area by using TB staining, which showed a significant increase in the cartilage matrix surrounding numerous chondrocytes in the hypertrophied LF, and that the percentage of the cartilage matrix area had a positive correlation with the LF thickness. These findings suggest that an increase in the number of chondrocytes and their cartilage matrix production are among the important factors in the mechanism of LF hypertrophy.

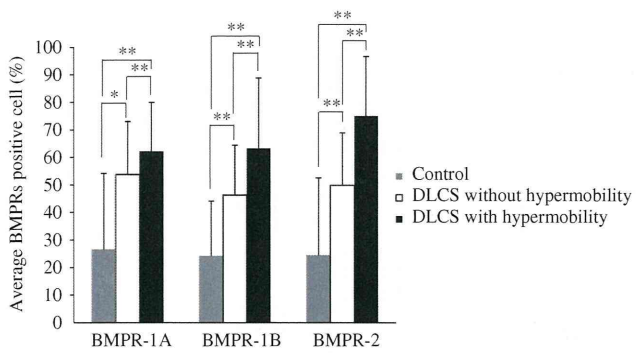

FIGURE 4. Percentages of cells positive for BMPR-1A, BMPR-1B, and BMPR-2 by immunohistochemistry. The percentage of cells positive for each BMPR is significantly higher in the DLCS with hypermobility group than in the DLCS without hypermobility group and the control group, and is also higher in the DLCS without hypermobility group than in the control group. *$P<0.05$; **$P<0.0001$. BMPR indicates bone morphogenetic protein receptors; DLCS, degenerative lumbar canal stenosis.

Although BMP signaling in the hypertrophied LF has received little attention, the immunohistochemical staining in this study showed that BMP and BMPR expressions were much higher in the hypertrophied LF. These immunopositive cells were observed not only among the increased chondrocytes, but also among fibroblast-like spindle cells and some round cells. Several earlier studies have shown that BMPs have great potential to induce chondrocyte differentiation and matrix production not only in mesenchymal stem cells, but also in ligament fibroblasts in vitro.[15,22–24] In addition, it has been reported that cultured bovine ligament fibroblasts express chondrocyte markers and produce cartilage matrix after stimulation by

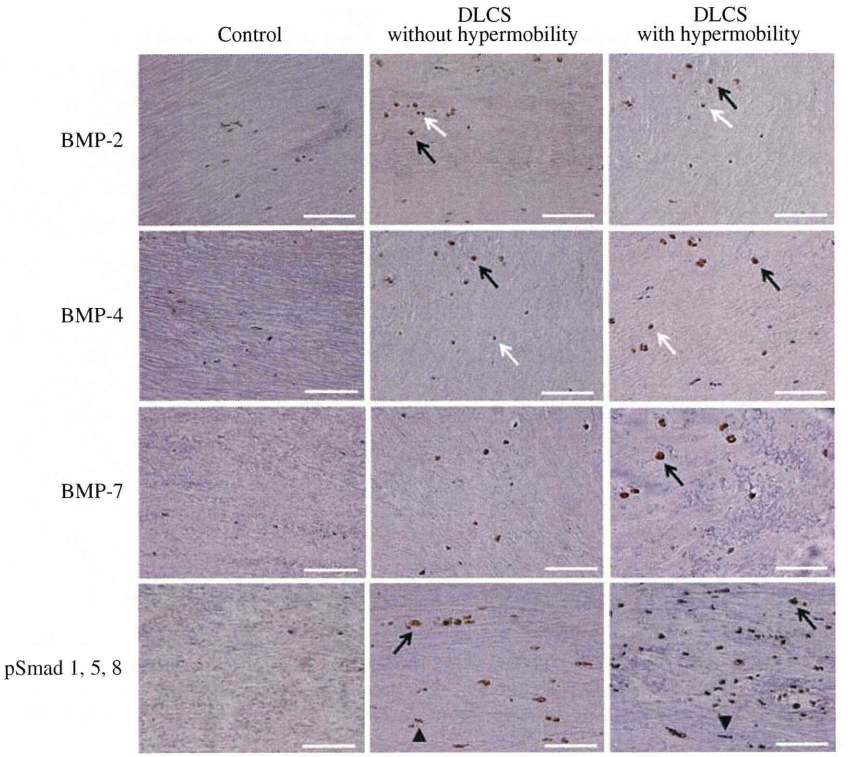

FIGURE 5. Immunohistochemistry for BMP-2, BMP-4, BMP-7, and phospho-Smad1/5/8 (×400; scale bars = 100 μm). Strong immunoreactivities are observed in the degenerative lumbar canal stenosis (DLCS) with hypermobility (right column) and without hypermobility groups (middle column), but only very weak immunoreactivity is observed in the control group (left column). Black arrows: hypertrophic chondrocytes; white arrows: immature chondrocytes; black arrowheads: fibroblast-like spindle cells. BMP indicates bone morphogenetic protein; DLCS, degenerative lumbar canal stenosis.

cartilage-derived morphogenetic protein-1 and protein-2, BMP-6, and BMP-7.[25] Hoshi et al[26] showed that recombinant human BMP-2 can induce endochondral ossification of the LF, and suggested that fibroblast-like cells in the LF can differentiate into chondrocytes or osteoblasts. Therefore, we considered that multipotent cells such as mesenchymal stem cells may exist in the LF tissue, and performed double and triple immunofluorescence staining for the markers CD105 (mesenchymal stem cell marker), Msx2 (hox gene family transcriptional factor required for the differentiation and proliferation of skeletogenic mesenchymal cells[27]), and Sox9 (chondrocyte

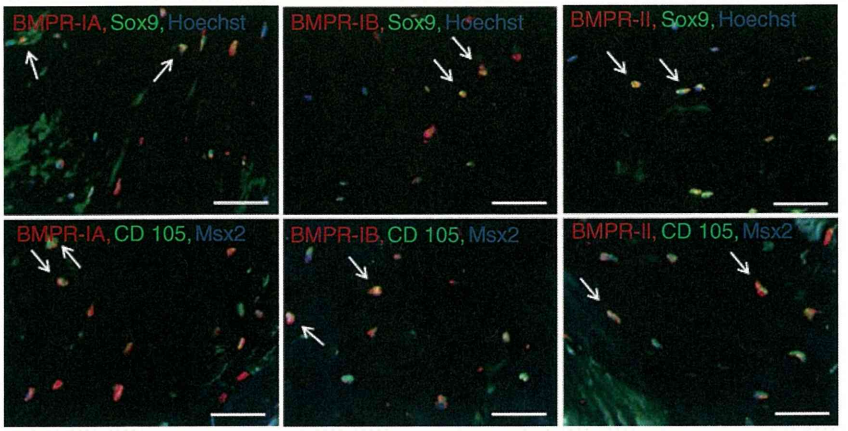

FIGURE 6. Immunofluorescence staining for BMPRs (red) and Sox9 (green) and nuclear counterstaining with Hoechst 33258 (blue) (top row) or immunofluorescence staining for BMPRs (red), CD105 (green), and Msx-2 (blue) (bottom row) in the hypertrophied ligamentum flavum (× 400; scale bars = 100 μm). Arrows indicate double-positive or triple-positive cells within the merged images. BMPR indicates bone morphogenetic protein receptors.

marker) combined with BMPR-1A, BMPR-1B, and BMPR-2. Our results showed that in the hypertrophied LF specimens, some cells positive for BMPRs coexpressed CD105, Msx2, and Sox9. Sox9 is known to be a transcription factor that plays important roles in both chondrogenic differentiation and cartilage matrix formation.[28] Considered together, these results suggest that BMP signaling partly contributes to the chondrogenic differentiation of immature cells or multipotent cells through an autocrine or a paracrine process during the development of LF hypertrophy in DLCS. However, the exact mechanism of chondrogenesis in the LF remains unclear, and further studies are required to clarify this issue.

In this study, we evaluated the influence of mechanical stress on the histology of LF specimens by using lumbar dynamic radiography. We showed that the cellularity and cartilage matrix area were significantly higher in the DLCS with hypermobility group than in the DLCS without hypermobility group. These observations suggest that mechanical stress plays a role in the process of LF hypertrophy through an increase in the cellularity or extracellular matrix production. It is well known that mechanical stress is converted to biochemical responses in various cells such as increases in gene expression and/or protein synthesis.[29] Several studies have shown similar phenomena for in vitro and in vivo chondrogenesis.[7,22,23] Huang et al[23] reported that mechanical stress increases TGF-β1 and collagen type 2 expressions in rabbit bone marrow mesenchymal stem cells. In addition, Nakatani et al[7] showed that mechanical stretching forces increase collagen synthesis and TGF-β1 production in cultured LF. In this study, we found that the percentages of cells immunopositive for BMPR-1A, BMPR-1B, and BMPR-2 were significantly higher in the DLCS with hypermobility group than in the DLCS without hypermobility group. These observations suggest that the BMP signaling may participate in the signal transduction from mechanical stress.

As with any investigation, our study had some limitations. First, the patients with DLCS were significantly older than the patients with LDH, and the sample size of the patients with LDH was smaller than that of the patients with DLCS. Therefore, we cannot exclude the possibility that natural aging processes or the affected levels had impacts on the variables measured in this study. Second, as we only evaluated the sagittal hypermobility by using dynamic lateral flexion-extension radiography, we could not refer to a specific mechanical stress, and it is possible that the hypermobility does not represent the real mechanical stress loading on the LF (c.f. coronal hypermobility). Finally, this was a histological observational study and could not show the exact roles of BMP signaling and mechanical stress in LF hypertrophy. However, given their known activities and roles, it is possible that these factors play some roles in the process of LF hypertrophy. To clarify the relevance of mechanical stress or the BMP signaling pathway in LF hypertrophy, in vivo animal studies or cell culture studies are required.

In conclusion, higher cellularity and increased cartilage matrix formation seemed to be significant underlying processes for LF hypertrophy, and these changes were more obvious in the DLCS with hypermobility group than in the DLCS without hypermobility group. These changes also showed significant positive correlations with the LF thickness. BMPRs and BMP ligands were expressed in many cells in the hypertrophied LF, including CD105-positive and Msx2-positive undifferentiated cells. These results suggest that mechanical stress and BMP signaling may play a role in LF hypertrophy through chondrogenesis and cartilage matrix production.

REFERENCES

1. Sairyo K, Biyani A, Goel VK, et al. Lumbar ligamentum flavum hypertrophy is due to accumulation of inflammation-related scar tissue. *Spine*. 2007;32:E340–E347.
2. Kosaka H, Sairyo K, Biyani A, et al. Pathomechanism of loss of elasticity and hypertrophy of lumbar ligamentum flavum in elderly patients with lumbar spinal canal stenosis. *Spine*. 2007;32:2805–2811.
3. Okuda T, Baba I, Fujimoto Y, et al. The pathology of ligamentum flavum in degenerative lumbar disease. *Spine (Philadelphia, PA 1976)*. 2004;29:1689–1697.
4. Schrader PK, Grob D, Rahn BA, et al. Histology of the ligamentum flavum in patients with degenerative lumbar spinal stenosis. *Eur Spine J*. 1999;8:323–328.
5. Yoshida M, Shima K, Taniguchi Y, et al. Hypertrophied ligamentum flavum in lumbar spinal canal stenosis. Pathogenesis and morphologic and immunohistochemical observation. *Spine*. 1992;17:1353–1360.
6. Fukuyama S, Nakamura T, Ikeda T, et al. The effect of mechanical stress on hypertrophy of the lumbar ligamentum flavum. *J Spinal Disord*. 1995;8:126–130.
7. Nakatani T, Marui T, Hitora T, et al. Mechanical stretching force promotes collagen synthesis by cultured cells from human ligamentum flavum via transforming growth factor-beta1. *J Orthop Res*. 2002;20:1380–1386.
8. Park JB, Chang H, Lee JK. Quantitative analysis of transforming growth factor-beta 1 in ligamentum flavum of lumbar spinal stenosis and disc herniation. *Spine*. 2001;26:E492–E495.
9. Sairyo K, Biyani A, Goel V, et al. Pathomechanism of ligamentum flavum hypertrophy: a multidisciplinary investigation based on clinical, biomechanical, histologic, and biologic assessments. *Spine*. 2005;30:2649–2656.
10. Gilboa L, Nohe A, Geissendorfer T, et al. Bone morphogenetic protein receptor complexes on the surface of live cells: a new oligomerization mode for serine/threonine kinase receptors. *Mol Biol Cell*. 2000;11:1023–1035.
11. Reddi AH. Bone morphogenetic proteins: from basic science to clinical applications. *J Bone Joint Surg Am*. 2001;83-A(suppl 1):S1–S6.
12. Zou H, Wieser R, Massague J, et al. Distinct roles of type I bone morphogenetic protein receptors in the formation and differentiation of cartilage. *Genes Dev*. 1997;11:2191–2203.
13. Rosen V, Thies RS, Lyons K. Signaling pathways in skeletal formation: a role for BMP receptors. *Ann N Y Acad Sci*. 1996;785:59–69.
14. Derynck R, Zhang YE. Smad-dependent and Smad-independent pathways in TGF-beta family signalling. *Nature*. 2003;425:577–584.
15. Palmer GD, Steinert A, Pascher A, et al. Gene-induced chondrogenesis of primary mesenchymal stem cells in vitro. *Mol Ther*. 2005;12:219–228.
16. Hayashi K, Ishidou Y, Yonemori K, et al. Expression and localization of bone morphogenetic proteins (BMPs) and BMP receptors in ossification of the ligamentum flavum. *Bone*. 1997;21:23–30.

17. Yonemori K, Imamura T, Ishidou Y, et al. Bone morphogenetic protein receptors and activin receptors are highly expressed in ossified ligament tissues of patients with ossification of the posterior longitudinal ligament. *Am J Pathol.* 1997;150:1335–1347.
18. Onishi T, Ishidou Y, Nagamine T, et al. Distinct and overlapping patterns of localization of bone morphogenetic protein (BMP) family members and a BMP type II receptor during fracture healing in rats. *Bone.* 1998;22:605–612.
19. Takae R, Matsunaga S, Origuchi N, et al. Immunolocalization of bone morphogenetic protein and its receptors in degeneration of intervertebral disc. *Spine.* 1999;24:1397–1401.
20. White AA, Panjabi MM. *The Problem of Clinical Instability in the Human Spine: A Systematic Approach, Part 4: the Lumbar and Lumbosacral Spine: Clinical Biomechanics of the Spine.* 2nd ed. New York: Lippincott Williams & Wilkins; 1990:342–361.
21. Iguchi T, Kanemura A, Kasahara K, et al. Lumbar instability and clinical symptoms: which is the more critical factor for symptoms: sagittal translation or segment angulation? *J Spinal Disord Tech.* 2004;17:284–290.
22. Elder SH, Fulzele KS, McCulley WR. Cyclic hydrostatic compression stimulates chondroinduction of C3H/10T1/2 cells. *Biomech Model Mechanobiol.* 2005;3:141–146.
23. Huang CY, Hagar KL, Frost LE, et al. Effects of cyclic compressive loading on chondrogenesis of rabbit bone-marrow derived mesenchymal stem cells. *Stem Cells.* 2004;22:313–323.
24. Steinert AF, Palmer GD, Pilapil C, et al. Enhanced in vitro chondrogenesis of primary mesenchymal stem cells by combined gene transfer. *Tissue Eng Part A.* 2009;15:1127–1139.
25. Bobacz K, Ullrich R, Amoyo L, et al. Stimulatory effects of distinct members of the bone morphogenetic protein family on ligament fibroblasts. *Ann Rheum Dis.* 2006;65:169–177.
26. Hoshi K, Amizuka N, Sakou T, et al. Fibroblasts of spinal ligaments pathologically differentiate into chondrocytes induced by recombinant human bone morphogenetic protein-2: morphological examinations for ossification of spinal ligaments. *Bone.* 1997; 21:155–162.
27. Ishii M, Merrill AE, Chan YS, et al. Msx2 and Twist cooperatively control the development of the neural crest-derived skeletogenic mesenchyme of the murine skull vault. *Development.* 2003; 130:6131–6142.
28. Bi W, Deng JM, Zhang Z, et al. Sox9 is required for cartilage formation. *Nat Genet.* 1999;22:85–89.
29. Chen CS. Mechanotransduction-a field pulling together? *J Cell Sci.* 2008;121:3285–3292.

Spine

SPINE Volume 36, Number 15, pp 1229–1235

DIAGNOSTICS

Characteristic Radiographic or Magnetic Resonance Images of Fresh Osteoporotic Vertebral Fractures Predicting Potential Risk for Nonunion

A Prospective Multicenter Study

Tadao Tsujio, MD,* Hiroaki Nakamura, MD, PhD,* Hidetomi Terai, MD, PhD,* Masatoshi Hoshino, MD, PhD,* Takashi Namikawa, MD, PhD,* Akira Matsumura, MD, PhD,* Minori Kato, MD, PhD,* Akinobu Suzuki, MD, PhD,* Kazushi Takayama, MD, PhD,* Wakaba Fukushima, MD, PhD,† Kyoko Kondo, PhD,† Yoshio Hirota, MD, PhD,† and Kunio Takaoka, MD, PhD,*

Study Design. Prospective multicenter study.

Objective. To identify radiographic or magnetic resonance (MR) images of fresh vertebral fractures that can predict a high risk for delayed union or nonunion of osteoporotic vertebral fractures (OVFs).

Summary of Background Data. Vertebral body fractures are the most common fractures in osteoporosis patients. Conservative treatments are typically chosen for OVFs, and associated back pain generally subsides within several weeks with residual persistent deformity of the vertebral body. In some patients, OVF healing is impaired and correlated with prolonged back pain. However, assessments such as plain radiograph or MR images taken during the early phase to predict high risks for nonunions of OVFs and/or poor prognoses have not been identified.

Methods. A total of 350 OVF patients from 25 institutes were enrolled in this clinical study. Plain radiograph and MR images of the OVFs were routinely taken at enrollment at the respective institutes. The findings on the plain radiograph and MR images were classified after enrollment in the study. All the patients were treated conservatively without any surgical intervention. After a 6-month follow-up, the patients were classified into two groups, a union group and a nonunion group, depending on the presence of an intravertebral cleft on plain radiograph or MR images. The associations of the images from the first visit with those of the corresponding nonunions at the 6-month follow-up were analyzed by multivariate logistic regression to elucidate specific image characteristics that may predict a high risk for nonunion of OVFs.

Results. Forty-eight patients (49 vertebrae) among the 350 patients (363 vertebrae) were classified as nonunions, indicating a nonunion incidence of 13.5% for conventional conservative treatments for OVFs. The statistical analyses revealed that a vertebral fracture in the thoracolumbar spine, presence of a middle-column injury, and a confined high intensity or a diffuse low intensity area in the fractured vertebrae on T2-weighted MR images were significant risk factors for nonunion of OVFs.

Conclusion. The results of this study revealed significant relationships between plain radiograph and MR images of acute phase OVFs and the incidence of nonunion. As these risk factors are defined more clearly and further validated, they may become essential assessment tools for determining subsequent OVF treatments. Patients with one or more of the earlier-described risk factors for nonunion should be observed carefully and provided with more intensive treatments.

Key words: MR images, nonunion, osteoporotic vertebral fractures, thoracolumbar spine, T2-weighted images. **Spine 2011;36: 1229–1235**

An increase in the number of osteoporosis-associated fractures is currently a major socioeconomic and medical problem in developed countries owing to the increasing population of elderly people.[1] To address this problem, various methods for treatment and/or prevention have been developed, but more efficacious ones would be advantageous in the coming decade.[2] In addition, vertebral fractures are the most common osteoporosis-related fractures with significant morbidity.[3] Symptomatically, severe back pain caused by such fractures gradually subsides with progression of bony union and spinal stability.[4,5] However, severe and intractable pain with[6] or without associated neurologic symptoms

From the *Department of Orthopaedic Surgery; and †Department of Public Health, Osaka City University Graduate School of Medicine, Osaka, Japan.

Acknowledgement date: October 2, 2010; Revision date: March 10, 2010; Acceptance date: June 28, 2010.

The manuscript submitted does not contain information about medical device(s)/drug(s).

Supported by grants from the Health and Labour Sciences Research Grants for Comprehensive Researach on Aging and Health, Japan.

No benefits in any form have been or will be received from a commercial party related directly or indirectly to the subject of this manuscript.

Address correspondence and reprint requests to Hiroaki Nakamura, MD, Department of Orthopaedic Surgery, Osaka City University Graduate School of Medicine, 1-4-3 Asahi-machi Abeno-ku, Osaka 545-8585, Japan; E-mail: hnakamura@med.osaka-cu.ac.jp

DOI: 10.1097/BRS.0b013e3181f29e8d

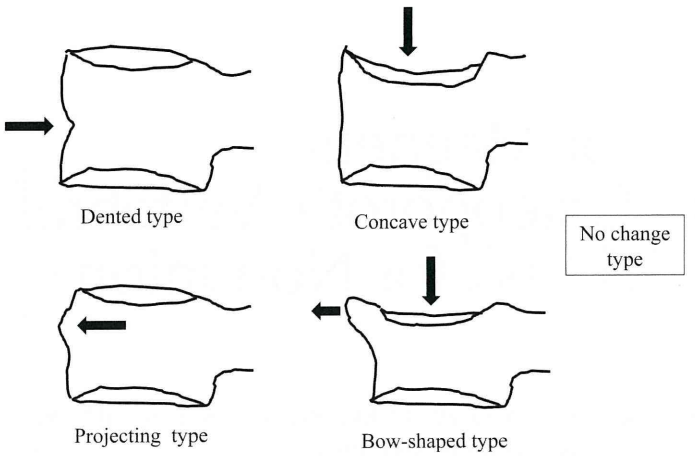

Figure 1. Types of fracture classified into five types based on Sugita's classification, as shown on lateral plain radiographs.

occasionally continues in a limited number of cases,[7] and these patients' activities of daily living (ADL) are markedly impaired.[8,9] Interestingly, radiograph and/or magnetic resonance (MR) images of their fractures frequently show characteristic and abnormal changes of nonunion, such as an intravertebral cleft sign on radiograms and/or a high signal band on T2-weighted MR images. The nonunion may, in part, be caused by insufficient early treatment and may be avoided by careful or intensive treatments other than bed rest or the use of a conventional brace. Unfortunately, screening of OVF patients with a high potential risk for a poor prognosis has not been clearly established for images of a fresh vertebral fracture. If characteristic signs, which are highly associated with a later nonunion, could be identified on radiographic or MR images, we may be able to screen patients with a high potential risk for nonunion and adjust their treatment accordingly to avoid a poor prognosis. Here, we performed a multicenter cohort study to identify radiograph or MR images of fresh vertebral fractures that can predict a high risk for delayed union or nonunion of OVFs.

MATERIALS AND METHODS

Patient Population

Twenty-five institutes in the Osaka area joined this prospective cohort study. Patients who were older than 65 years and had a fresh OVF were enrolled in this study after written informed consent was obtained. On the initial visit to the respective institutes, a fresh vertebral fracture was diagnosed by acute back pain, a deformed vertebral body on radiograms and an abnormal intensity within the vertebral bodies on MR images. The study design was pre-approved by the Ethical Committee for Clinical Research at the respective institutes.

A total of 485 patients were enrolled. Of these, 15 patients died, 11 were excluded because of other diseases and 39 patients were lost to follow-up. As a result, 420 patients completed the 6-month follow-up (86.6% follow-up rate). Among these 420 patients, 350 patients (363 vertebral fractures in 54 men and 296 women) with all of the required data including examinations and completed questionnaires at both the times of the enrollment and the 6-month follow-up were included in the present study. The age at the time of enrollment ranged from 65 to 93 years, with a mean age of 75.9 years.

At the time of enrollment, the patients were examined by plain radiograph and MR imaging of the spine. The calcaneal bone quality was evaluated by a speed of sound (SOS) parameter in quantitative ultrasound measurements. The severity of pain was assessed subjectively by the patients with a visual analogue scale (VAS), in which the scale was assessed by the average level of back pain that the patient had felt in the previous 1 week. At the 6-month follow-up, all the patients were re-examined by plain radiograph and MR imaging. The severity of pain was also reassessed with the VAS score.

Overall, 240 patients were hospitalized for several days during the acute phase and 110 were outpatients. At treatments, 65 patients wore tailor-made hard corsets, 180 wore tailor-made elastic corsets, 69 wore ready-made elastic corsets, and 36 did not wear a corset. These treatment options were decided by the individual physicians based on their experience. All of the physicians were specialist orthopedic surgeons. Therefore, we considered that the treatment options,

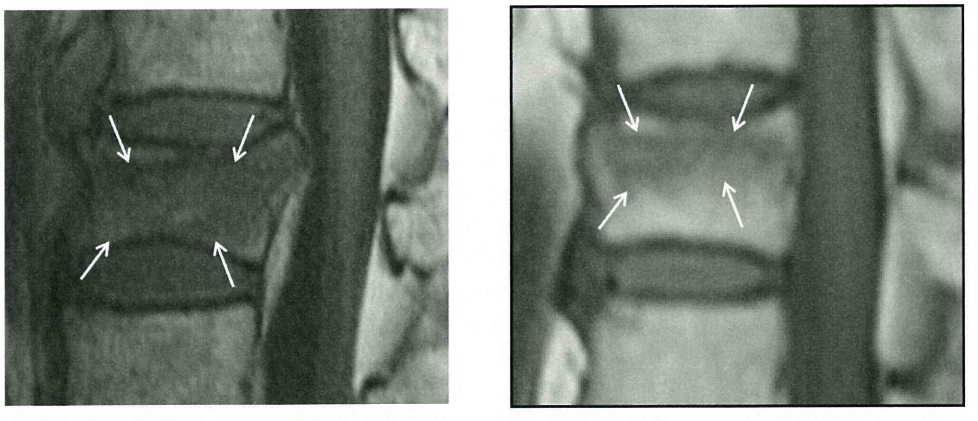

Figure 2. Intensity changes of the fractured vertebral bodies on T1-weighted images were classified into two patterns: diffuse low intensity type and confined low intensity type.

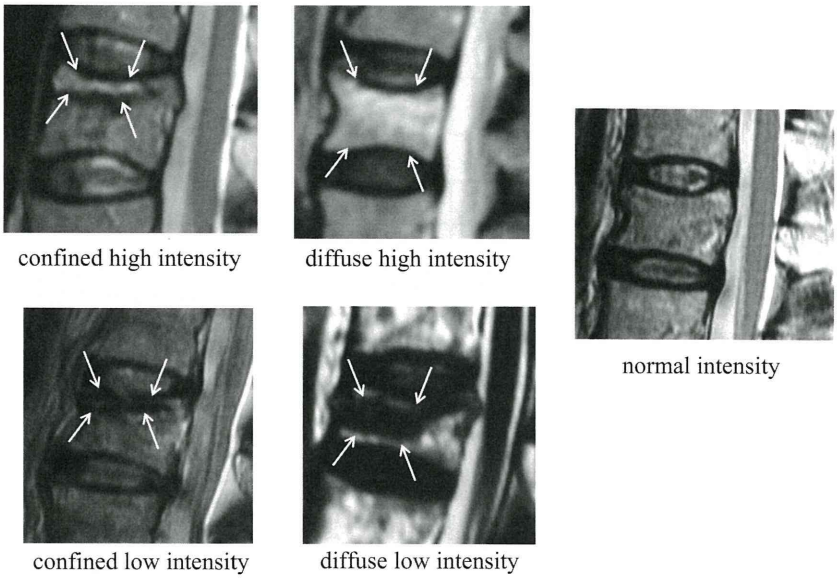

Figure 3. Intensity changes of the fractured vertebral bodies on T2-weighted MR images were classified into five patterns: confined high intensity type, diffuse high intensity type, confined low intensity type, diffuse low intensity type, and normal intensity.

including the use of a brace, were standard treatments for OVFs at the time of enrollment in Japan.

Imaging Parameters

At the time of enrollment, the findings on plain radiograph and MR images were assessed by three independent physicians. Regarding the plain radiograph images, the vertebral fractures were classified into one of five types on lateral plain radiograms according to Sugita's classification (Figure 1).[10]

The patterns of intensity changes within fractured vertebral bodies on MR images were classified on both midsagittal T1- and T2-weighted images. The intensity changes on T1-weighted images were classified into two patterns: diffuse low intensity type and confined low intensity type (Figure 2). The intensity changes on T2-weighted images were classified into five patterns: confined high intensity type, diffuse high intensity type, confined low intensity type, diffuse low intensity type and normal intensity (Figure 3). Damage to the middle column, as evidenced by protrusion of the posterior wall of the vertebral body into the spinal canal, was also evaluated on midsagittal MR images.

At the time of the 6-month follow-up, three independent physicians classified the cases into two groups, a union group and a nonunion group, with blinding to the initial image findings. Nonunion was defined by a recognizable intravertebral cleft on plain radiograph images (Figure 4). The percentages of nonunion were calculated for the two classification groups based on the findings on plain radiograph and MR images at the time of enrollment.

Statistical Analysis

Differences between the two groups were assessed by a t test, the Wilcoxon rank sum test for continuous variables or the χ^2 test for categorical variables. To elucidate the prognostic risk factors for nonunion, a multivariate statistical analysis was performed. Odd ratios (ORs) for nonunion occurrences and their 95% confidence intervals (CIs) were calculated as an approximation of the relative risk estimates. The factors included in the multivariate model were age, sex, body mass index and those with a value of $P < 0.05$ in the univariate analyses, as well as clinically important variables (*i.e.*, type of corset used, bone mineral density, presence of prevalent vertebral fractures) regardless of their statistical significance. Nonunion as determined by radiograms was defined as a response variable. All statistical analyses were conducted using SAS version 9.1 (SAS Institute Inc, Cary, NC). A value of $P < 0.05$ was considered to be statistically significant.

Figure 4. Vertebral body exhibiting an intravertebral cleft, defined as nonunion, after an OVF.

TABLE 1. Demographic Data and VAS Scores of the Patients in the Two Groups

	Union	Nonunion	
	No. (%) or Mean ± SD		
Vertebrae	314	49	
Age (years)	75.7 ± 6.5	77.3 ± 6.4	NS
BMD (m/s)	1473.9 ± 23.8	1473.1 ± 20.5	NS
Prevalent fractures	117 (38.7)	23 (47.9)	NS
VAS score the time of enrollment	8.2 ± 2.0	8.7 ± 1.7	NS
The time of the 6-mo follow-up	3.0 ± 2.5	3.9 ± 2.5	$P = 0.032$

NS indicates not significant.

RESULTS

Radiograms of satisfactory bony unions, without associated severe pain, were obtained in 302 patients (314 vertebrae) at the 6-month follow-up. These cases were included in the union group. Forty-eight patients (49 vertebrae) who showed cleft signs on lateral radiograph images were assigned to the nonunion group. Consequently, the incidence of nonunion of the vertebral fractures treated by conventional nonsurgical methods for 6 months was estimated to be 13.5%. The ages at the time of enrollment were 75.7 ± 6.5 years in the union group and 77.3 ± 6.4 years in the nonunion group, with no significant difference. The SOS values on the quantitative ultrasound measurements were 1473.9 ± 23.8 and 1473.1 ± 20.5 m/s in the union and nonunion groups, respectively. Prevalent fractures were noted in 38.7% of patients in the union group and 47.9% of patients in the nonunion group. These values did not differ significantly between the two groups (Table 1).

The VAS scores for back pain improved from 8.2 ± 2.0 to 3.0 ± 2.5 in the union group and from 8.7 ± 1.7 to 3.9 ± 2.6 in the nonunion group at the 6-month follow-up. The VAS values at the 6-month follow-up were significantly higher in the nonunion group than in the union group (Table 1).

The distributions of the levels of the OVFs are shown in Figure 5. The majority of the fractures were located at the thoracolumbar junction, predominantly at L1. However, nonunion was most frequently observed at T12. The initial fracture types did not differ significantly in the union or nonunion groups (Table 2). There were no substantial pattern differences in the union or nonunion groups according to the T1-weighted MR image patterns (Table 3). The confined high intensity type and diffuse low intensity type image patterns on T2-weighted images were frequently observed in the nonunion group (52.9% and 26.6% of patients, respectively) (Table 4).

To identify potential risk factors for nonunion according to univariate analyses, high ORs were found when there were confined high intensity changes or diffuse low intensity changes within the vertebral body on T2-weighted images (OR = 31.7, 95% CI = 12.4–81.1, $P < 0.001$ and OR = 9.7, 95% CI = 4.2–22.2, $P < 0.001$, respectively). Notably, the presence of a middle-column injury, involvement at the thoracolumbar vertebrae, and bony fusion in the adjacent

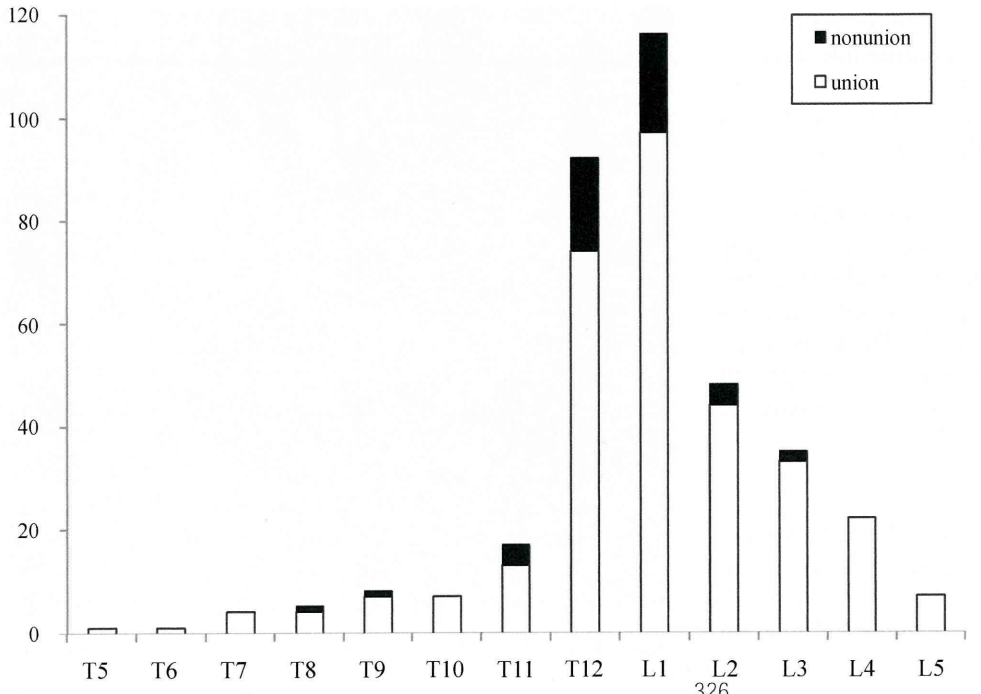

Figure 5. Distributions of the levels of the OVFs and those of nonunion cases.

TABLE 2. Occurrences of Nonunion According to the Fracture Patterns on Plain X-ray Images

Type	No. of Vertebral Fracture	Nonunion Occurrence, (%)
No change	25	2 (8.0)
Dented	21	2 (9.5)
Concave	61	6 (9.8)
Projecting	56	7 (12.5)
Bow-shaped	200	32 (16.0)

TABLE 4. Occurrences of Nonunion According to the Intensity Changes on T2-Weighted MR Images

Type	No. of Vertebral Fracture	Nonunion Occurrence, (%)
Normal	25	0 (0)
Confined high	34	18 (52.9)
Diffuse high	21	1 (4.8)
Confined low	204	9 (4.4)
Diffuse low	79	21 (26.6)

segments also exhibited significantly high ORs (OR = 4.3, 95% CI = 1.5–12.3, $P < 0.01$; OR = 4.2, 95% CI = 2.2–7.8, $P < 0.001$; and OR = 2.6, 95% CI = 1.1–6.0, $P = 0.02$, respectively).

A multivariate regression analysis revealed high ORs for the confined high intensity patterns and diffuse low intensity patterns on T2-weighted images (OR = 32.3, 95% CI = 11.0–94.9, $P < 0.001$ and OR = 6.8, 95% CI = 2.5–18.3, $P < 0.001$, respectively). Middle-column damage and thoracolumbar level involvement also exhibited significantly increased ORs for nonunion (OR = 3.5, 95% CI = 1.4–8.4, $P < 0.006$ and OR = 5.1, 95% CI = 1.4–18.1, $P < 0.01$, respectively). No other examined variables were significant risk factors for nonunion according to the multivariate analysis (Table 5). The percentages of nonunion cases with these risk factors and with two or three of these risk factors are shown in Table 6. Patients with two or all the three risk factors were at greater risk of nonunion.

DISCUSSION

This prospective clinical study was designed to identify characteristic radiographic and/or MR images for the acute phase of OVFs that may predict a high risk for nonunion by comparing fresh fracture images from a nonunion patient group with those in a union group after a 6-month follow-up. The incidence of nonunion in this study was 13.5%, which was similar to the incidences in previous reports,[11] indicating limited outcomes for the conventional treatment methods for OVFs. To improve the clinical outcome, screening for potential high risk factors associated with nonunion would be important.

TABLE 3. Occurrences of Nonunion According to the Intensity Changes on T1-Weighted MR Images

Type	No. of Vertebral Fracture	Nonunion Occurrence, (%)
Confined	93	6 (6.5)
Diffuse	270	43 (15.9)

At the 6-month follow-up, the presence of a cleft with frequent intravertebral vacuum signs within the fractured vertebra on the lateral radiographic view was adopted as the criterion for defining nonunion. This pathologic change is frequently associated with spinal instability, which is recognized on a dynamic lateral radiogram, and causes prolonged back pain that is typically aggravated by standing or walking. A vertebra with nonunion occasionally leads to delayed-onset collapse[6,12,13] with the development of neurologic symptoms.[6] To avoid such nonunions after vertebral fractures, identifying specific signs, or image patterns during the acute phase that can be used to predict a high risk for nonunion is essential for the development of new and efficacious treatments for these patients. However, few reports have described such predictive risk factors for nonunion.

On the basis of the results of the present study, potential high risk factors for nonunion were found for two T2-weighted MR image patterns: high intensity confined to a partial zone within the fractured vertebra and a diffuse low intensity pattern within the vertebra. The grades of the potential risk (ORs) of these T2-weighted image patterns calculated by a multivariate regression analysis were extremely high (32.3 and 6.8, respectively). Although the pathologic mechanism of the high incidences of fracture nonunion associated with these T2-weighted MR image patterns could not be elucidated in this study, it is possible that concentrated and repeated mechanical compression and tensile and shear stresses to the fracture site are characterized by the confined high intensity on the T2-weighted images within the vertebrae, causing prolonged instability, and impaired repair of the fracture. Extensive damage to the vertebrae may also result in fibrosis owing to excessive instability, which deters new bone formation and leads to nonunion, and this type of damage may contribute to the diffuse low intensity patterns in vertebrae on T2-weighted images. Clearly, further studies are necessary to understand the significance of the specific MR image patterns in association with the risks for nonunion.

Damage to the middle column was also identified as a risk factor for nonunion in this study (OR = 3.5). Wu *et al*[14] previously reported that fractures involving both the anterior and

TABLE 5. Prognostic factors for the occurrence of non-union

	Univariate		Multivariate*	
	OR (95% CI)	*P* Value	OR (95% CI)	*P* Value
MRI T2				
Confined high	31.7 (12.4–81.1)	< 0.001	32.4 (11.0–94.9)	< 0.001
Diffuse low (*vs.* No change, diffuse high, confined low)	9.7 (4.2–22.2)	< 0.001	6.8 (2.5–18.3)	< 0.001
Middle column injury (*vs.* absence)	4.1 (2.2–7.8)	< 0.001	3.5 (1.4–8.4)	0.006
Thoracolumbar level (*vs.* absence)	4.3 (1.5–12.3)	0.006	5.1 (1.4–18.1)	0.013
Vertebral fusion at the adjacent segments (*vs.* absence)	2.6 (1.1–6.0)	0.024	1.6 (0.5–4.8)	0.451

OR = odds ratio; CI = confidence interval.

**The multivariate model included age, sex, body mass index, type of corset, bone mineral density, presence, or absence of prevalent fracture and all the variables listed in the table.*

middle columns were associated with a higher incidence of nonunion than those involving the anterior column alone. However, the two MR image patterns indicated a much higher OR than that for middle-column damage in the present study.

We believe that fresh vertebral fractures that have a potential risk for nonunion according to their MR or radiograph images should undergo careful observation and treatment. Less invasive surgical procedures, such as vertebroplasty with injected bone cement,[15–17] may be alternative treatments for fresh vertebral fractures with such high-risk image patterns because of the rapid pain relief.[18–20] However, further investigations are needed to determine whether the findings of the current study can lead to improved outcomes by altering the treatment choices based on the radiographic risk factors for nonunion.

TABLE 6. Occurrences of Nonunion According to the Risk Factors

	No. of Vertebral Fracture	Nonunion Occurrence, (%)
Thoracolumbar level (TLL)		
Yes	272	45 (16.5)
No	91	4 (4.4)
Middle column injury (MCI)		
Presence	110	29 (26.4)
Absence	253	20 (7.9)
TLL + MCI	93	27 (29.0)
TLL + MCI + MRI T2	13	10 (76.9)
Confined high		
TLL + MCI + MRI T2	40	14 (35.0)
Diffuse low		

CONCLUSIONS

The rate of nonunion after OVF was 13.5% in the present prospective study. Fracture at the thoracolumbar level, middle-column injury and confined high intensity or diffuse low intensity changes on T2-weighted MR images were predictive factors for nonunion (with the latter two exhibiting the highest ORs). These findings should be useful for predicting the prognosis of OVFs.

➢ Key Points

- ❑ The incidence of nonunion in osteoporotic vertebral fractures in the elderly was 13.5% in this study after 6 months of conventional conservative treatments.
- ❑ Among the radiographic and MR images, images showing a significant risk for nonunion were screened by a multivariate regression analysis.
- ❑ The risk factors in these images were (1) a fracture in the thoracolumbar spine, (2) the presence of a middle-column injury, and (3) a confined high intensity or a diffuse low intensity area on a T2-weighted MR image.

Acknowledgments

The authors thank Masami Tatsumi, Tomomi Tanaka, Tomoko Komaru, Aki Tanaka, Asami Satou, and Keiko Yoneda for their help in the collection of data and interviews with the patients. The authors also thank the physicians from Osaka City General Hospital, Osaka City Juso Hospital, Osaka City Kita Hospital, Osaka City Sumiyoshi Hospital, Kousaiin Hospital, Hujiidera Municipal Hospital, Izumi Municipal Hospital, Aeba Surgical Hospital, Yodogawa Christian Hospital, Ishikiri Seiki Hospital, Asakayama Hospital, Osaka Ekisaikai Hospital, Kyouwa Hospital, Saiseikai Nakatsu Hospital, Saiseikai Senri Hospital, Baba Memorial Hospital, Seikeikai Hospital, Nagayoshi Sougou Hospital, Nishinomiya Watanabe Hospital, Hankai Hospital, Higashisumiyoshi Morimoto Hospital,

Shitennoji Hospital, Satou Hospital, and Tsujigeka Hospital for enrolling the patients in this prospective study. The authors thank the grants from the Health and Labour Sciences Research Grants for Comprehensive Research on Aging and Health of Japan.

References

1. Cummings SR, Melton LJ. Epidemiology and outcomes of osteoporotic fractures. *Lancet* 2002;359:1761–7.
2. Fujiwara S. Epidemiology of osteoporosis in Japan. *J Bone Miner Metab* 2005;23 Suppl:81–3.
3. Ross PD, Fujiwara S, Huang C, et al. Vertebral fracture prevalence in women in Hiroshima compared to Caucasians or Japanese in the US. *Int J Epidemiol* 1995;24:1171–7.
4. Itoi E, Sakurai M, Mizunashi K, et al. Long-term observations of vertebral fractures in spinal osteoporotics. *Calcif Tissue Int* 1990;47:202–8.
5. Lee YL, Yip KM. The osteoporotic spine. *Clin Orthop Relat Res* 1996:91–7.
6. Ito Y, Hasegawa Y, Toda K, et al. Pathogenesis and diagnosis of delayed vertebral collapse resulting from osteoporotic spinal fracture. *Spine J* 2002;2:101–6.
7. Hasegawa K, Homma T, Uchiyama S, et al. Vertebral pseudarthrosis in the osteoporotic spine. *Spine* 1998;23:2201–6.
8. Ensrud KE, Thompson DE, Cauley JA, et al. Prevalent vertebral deformities predict mortality and hospitalization in older women with low bone mass. Fracture Intervention Trial Research Group. *J Am Geriatr Soc* 2000;48:241–9.
9. Silverman SL, Minshall ME, Shen W, et al. The relationship of health-related quality of life to prevalent and incident vertebral fractures in postmenopausal women with osteoporosis: results from the Multiple Outcomes of Raloxifene Evaluation Study. *Arthritis Rheum* 2001;44:2611–9.
10. Sugita M, Watanabe N, Mikami Y, et al. Classification of vertebral compression fractures in the osteoporotic spine. *J Spinal Disord Tech* 2005;18:376–81.
11. Kim DY, Lee SH, Jang JS, et al. Intravertebral vacuum phenomenon in osteoporotic compression fracture: report of 67 cases with quantitative evaluation of intravertebral instability. *J Neurosurg* 2004;100:24–31.
12. Hashidate H, Kamimura M, Nakagawa H, et al. Pseudoarthrosis of vertebral fracture: radiographic and characteristic clinical features and natural history. *J Orthop Sci* 2006;11:28–33.
13. Kaneda K, Asano S, Hashimoto T, et al. The treatment of osteoporotic-posttraumatic vertebral collapse using the Kaneda device and a bioactive ceramic vertebral prosthesis. *Spine* 1992;17:S295–303.
14. Wu CT, Lee SC, Lee ST, et al. Classification of symptomatic osteoporotic compression fractures of the thoracic and lumbar spine. *J Clin Neurosci* 2006;13:31–8.
15. Alvarez L, Alcaraz M, Perez-Higueras A, et al. Percutaneous vertebroplasty: functional improvement in patients with osteoporotic compression fractures. *Spine* 2006;31:1113–8.
16. Galibert P, Deramond H, Rosat P, et al. Preliminary note on the treatment of vertebral angioma by percutaneous acrylic vertebroplasty [in French]. *Neurochirurgie* 1987;33:166–8.
17. Jensen ME, Evans AJ, Mathis JM, et al. Percutaneous polymethylmethacrylate vertebroplasty in the treatment of osteoporotic vertebral body compression fractures: technical aspects. *AJNR Am J Neuroradiol* 1997;18:1897–904.
18. Barr JD, Barr MS, Lemley TJ, et al. Percutaneous vertebroplasty for pain relief and spinal stabilization. *Spine* 2000;25:923–8.
19. Kasperk C, Hillmeier J, Nöldge G, et al. Treatment of painful vertebral fractures by kyphoplasty in patients with primary osteoporosis: a prospective nonrandomized controlled study. *J Bone Miner Res* 2005;20:604–12.
20. McKiernan F, Faciszewski T, Jensen R. Quality of life following vertebroplasty. *J Bone Joint Surg Am* 2004;86-A:2600–6.

Arch Orthop Trauma Surg (2011) 131:59–64
DOI 10.1007/s00402-010-1102-7

ORTHOPAEDIC SURGERY

Evaluation of clinical problems associated with bone metastases from carcinoma from unknown primary sites

Manabu Hoshi · Susumu Taguchi · Keiko Hayakawa · Makoto Ieguchi · Hiroaki Nakamura

Received: 10 December 2009 / Published online: 22 April 2010

Abstract
Introduction This study focused on the evaluation of data concerning the clinical features of patients who were initially diagnosed with bone metastases of carcinoma from unknown primary sites that could not be detected, even using state of-the-art diagnostic modalities.
Method The oncologic outcome of these patients is discussed.
Patients The clinical records of seven patients who had presented with bone metastases of carcinoma from unknown primary sites were retrospectively reviewed. Clinical features, treatment and outcome were analyzed. Extraskeletal metastases were located in the lymph nodes, liver, skeletal muscle, kidney, adrenal gland, and pleura. Six cases were observed in the pelvis, three in the femur, three in the skull, two in the rib, two in the cervical spine, two in the thoracic spine, two in the lumbar spine, one in the humerus, one in the radius, one in the clavicle, one in the scapula and one in the sternum. Four patients received systemic chemotherapy including platinum.
Results At the last follow-up time of average 272 days, six patients were dead of disease and one patient was alive with disease. Although considerable progress has been made in the development of diagnostic modalities, including more recently FDG-PET, the primary tumor site cannot always be identified. Multiple bone and visceral organ metastases are often present in patients whose primary tumor was not detected.
Conclusion In the present study, it was found that systemic chemotherapy can appreciably increase the survival time of the patients with carcinoma metastases from unknown primary sites.

Keywords Unknown primary site · Bone metastasis · Treatment · Chemotherapy

M. Hoshi (✉) · S. Taguchi · K. Hayakawa · M. Ieguchi · H. Nakamura
Department of Orthopedic Surgery,
Osaka City University Graduate School of Medicine,
1-4-3 Asahi-machi, Abeno-ku, Osaka 545-8585, Japan
e-mail: hoshi@med.osaka-cu.ac.jp

Introduction

The prognosis of patients with various types of carcinoma has been gradually improved due to early diagnosis using modern imaging techniques and improved treatment protocols. Because of higher control rates of the primary tumor in recent decades, the prolonged survival of patients has significantly increased the risk of developing distant metastases. Carcinoma metastasis from unknown primary sites is frequently detected in the lymph nodes due to swelling [1] and bone is also a frequent target site. 10–15% of patients present with symptoms of occult cancer [2].

Identification of the primary site is critical in enabling a rapid start to treatment. Unfortunately, even with the recent progress in the development of variable diagnostic techniques, the primary tumor site cannot be determined always. Failure to locate the primary tumor using multimodal diagnostic approaches leads to increased treatment delays and costs. As a consequence, patients cannot undergo cancer-specific treatment and their overall prognosis is generally poor.

In the present study, the clinical features and oncological outcomes of a group of patients treated for carcinoma metastases in the bone were examined. Only patients whose primary site of carcinoma could not be detected using the latest diagnostic modalities were admitted into the study.

Patients in whom the primary location of the carcinoma could be identified were excluded.

Materials and methods

From March 1994 to 2009, seven patients with carcinoma metastases in the bone were treated and followed up. All patients were evaluated with physical examinations, various radiological evaluations and pathological investigation using biopsy. The primary site of the carcinoma in these patients could not be identified. There were three male and four female patients, with a mean age at diagnosis of 61.9 years (range 49–80 years), were followed up for a median period of 272 days (range 16–469 days). No patient was lost during follow-up. The clinical information reviewed in this study included performance status, laboratory date of tumor marker [alkaline phosphatase (ALP), lactate dehydrogenase (LDH), carcinoembryonic antigen (CEA)], anatomical site of bone metastases or extraskeletal metastases, histology and treatment modalities. Oncologic outcome at the last follow-up was also examined.

Results

The characteristics of patients with bone metastases from carcinoma originating from unknown primary sites are summarized in Table 1. At their first visit to our orthopedic department, the performance status was zero in two patients, one in two patients, two in one patient and three in two patients. Laboratory data showed elevated levels of ALP in five out of seven patients, LDH in four out of seven patients and CEA in four out of seven patients. Radiological imaging of patients, including FDG-PET, revealed that extraskeletal metastases were located in the lymph nodes in five cases (Fig. 1a), liver in two cases, skeletal muscle of the buttock in two cases (Fig. 1b, c), lower leg in two cases, kidney in one case, adrenal gland in one case and pleura in one case.

The incidence of bone metastases at different sites and the oncologic outcome of patients are summarized in Table 2. There were six cases of bone metastases in the pelvis (Fig. 1b, c), three in the femur, three in the skull, two in the ribs, two in the cervical spine, two in the thoracic spine, two in the lumbar spine, two in the humerus, one in the radius, one in the clavicle, one in the scapula and one in the sternum.

For histopathological diagnosis, six patients were biopsied. One patient underwent endoprosthetic replacement (Fig. 2a, b). Biopsy specimens and surgical specimens were identified as adenocarcinoma in three patients (Fig. 3a),

Table 1 Characteristics of patients with bone metastases from carcinoma of primary unknown site

		Number	%
Age	61.9 (mean)		
PS	0	2	28.6
	1	2	28.6
	2	1	14.3
	3	2	28.6
	4	0	
Laboratory			
ALP	Elevated	5	71.4
LDH	Elevated	4	57.1
CEA	Elevated	4	57.1
Extraskeletal metastases			
Lymph node		5	71.4
Liver		2	28.6
Kidney		1	14.3
Skeletal muscle		2	28.6
Adrenal gland		1	14.3
Pleura		1	14.3

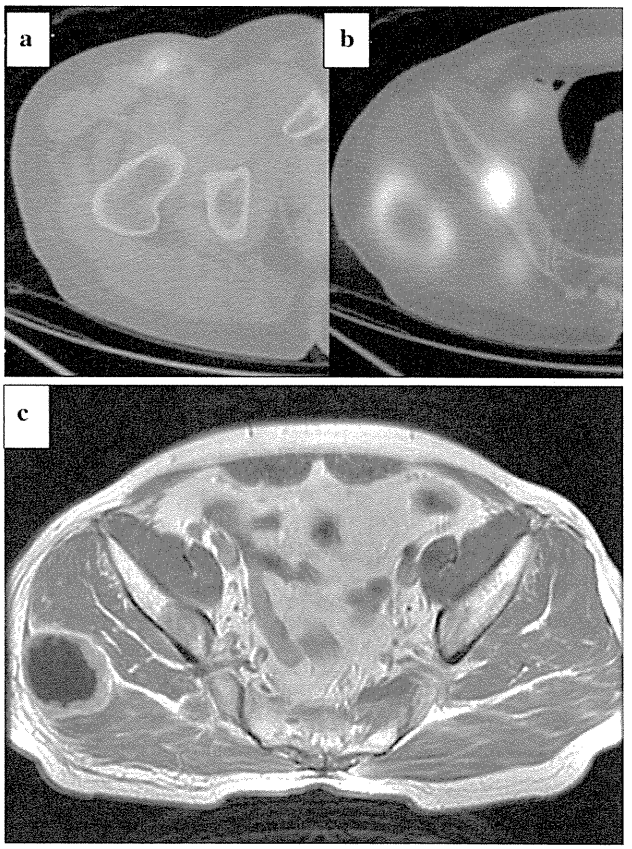

Fig. 1 Case 1. **a** PET/CT shows the lymph node swelling in the right inguinale. **b** PET/CT demonstrates the abnormal uptakes in intrapelvic lymph node, ilium, and buttocks. **c** Axial T2 weighted MRI shows the bone metastases of the right ilium and soft tissue metastasis in buttock

Table 2 Bone metastases and oncologic outcome in carcinoma of unknown primary sites

Case	Age	Sex	Histology	Bone metastasis	Treatment	Follow-up (days)	Prognosis
1	54	M	Adenocarcinoma	Pelvis	CT (CBDCA + PTX, TS1), RT (pelvis)	131	AWD
2	75	F	Adenocarcinoma	Skull, rib, pelvis, thoracic	RT (pelvis, thoracic)	407	DOD
3	55	F	Adenocarcinoma	Femur, pelvis, clavicle	CT (TS1), surgery (femur)	469	DOD
4	49	M	Poorly differentiated carcinoma	Femur	RT (femur)	33	DOD
5	64	F	Signet ring cell carcinoma	Skull, cervix, lumbar, thoracic, rib, pelvis	CT (CBDCA + PTX)	420	DOD
6	80	F	Poorly differentiated carcinoma	Carpal, lumbar, pelvis	RT (pelvis)	16	DOD
7	56	M	Signet ring cell carcinoma	Scapula, sterunum, pelvis, femur, skull, cervix, lumbar, humerus	CT (CBDCA + PTX, TS1 + GEM)	429	DOD

RT Radiation therapy, *CT* Chemotherapy, *CBDCA* carboplatin, *PTX* paclitaxel, *GEM* gemcitabine hydrochloride, *DOD* Die of disease, *AWD* Alive with disease

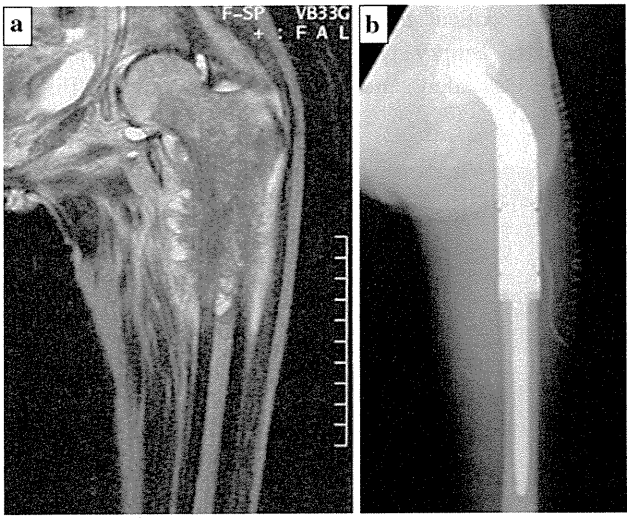

Fig. 2 Case 3. **a** Coronal T2 view of MRI shows the bone metastases of proximal femur. **b** Plain film shows the endoprosthetic replacement after tumor resection

signet ring cell carcinoma in two patients (Fig. 3b) and poorly undifferentiated carcinoma in two patients (Fig. 3c).

After diagnosis of metastatic cancer, three patients had major health problems. Two patients were in frail health, due to age (cases 2 and 6). One patient (case 4) had severe chronic renal failure. Four patients (cases 1, 3, 5 and 7) received systemic chemotherapy, and their regimen consisted of three sessions of carboplatin (CBDCA). The median survival time was 429 days for patients receiving chemotherapy, and 33 days for patients that did not undergo chemotherapy.

Three patients received local radiation therapy. One patient (case 3) showed prominent sclerotic changes after radiation therapy, indicating efficacy in treating the cancer (Fig. 4). In another patient (case 6), health suddenly deteriorated during radiation treatment and death followed after 10 days. At an average follow-up time of 272 days, six patients were DOD and only one patient was AWD. The median survival time of all patients was 420 days.

Discussion

Carcinoma metastases originating from an unknown primary site have been defined by Pavlidis et al. [3] as cancer occurring in patients who present with histologically confirmed metastatic disease, in whom a detailed medical history, complete physical examination, histopathological review of biopsy material with use of immunohistochemistry, chest radiography, CT of abdomen and pelvis failed to identify the primary site. The incidence of carcinoma metastases from unknown primary sites is approximately 3% of all malignant neoplasms. The common sites of occurrence of these metastases are the lymph nodes, liver, lung and bone [1].

Patients with bone metastases are often referred to an orthopedic oncologist by general physicians for investigation of the location of the primary tumor site. There is a need to identify the primary site as quickly as possible, in order to finalize the diagnosis and begin treatment. The incidence of carcinoma metastases in bone originating from unknown primary sites in the gastro-intestinal tract is relatively low. However, lung, prostate and breast cancer metastases occur more frequently in bone. As a consequence, endoscopy of the digestive tract is not the first choice for the primary investigation [4, 5]. This is due to the fact that it is neither time- nor cost-effective to do so and can delay treatment.

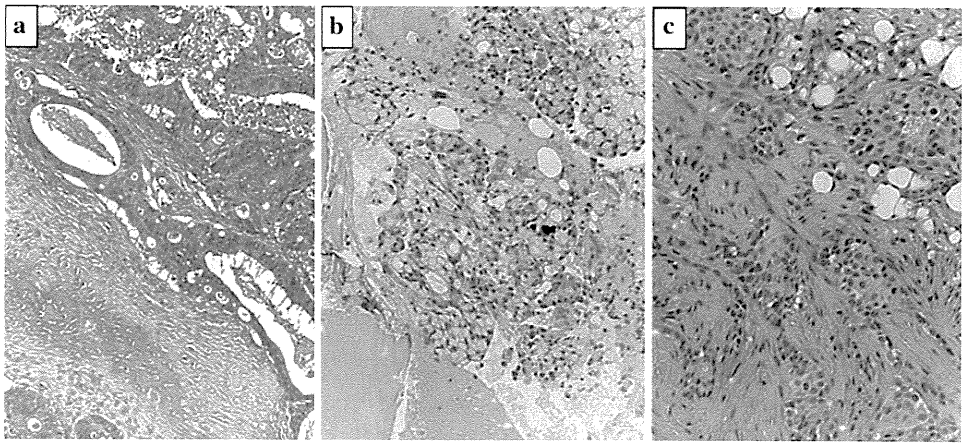

Fig. 3 **a** Histopathology confirms adenocarcinoma (Case 3), **b** signet ring cell carcinoma (Case 5), and **c** poorly differentiated carcinoma (Case 6) (magnification ×200)

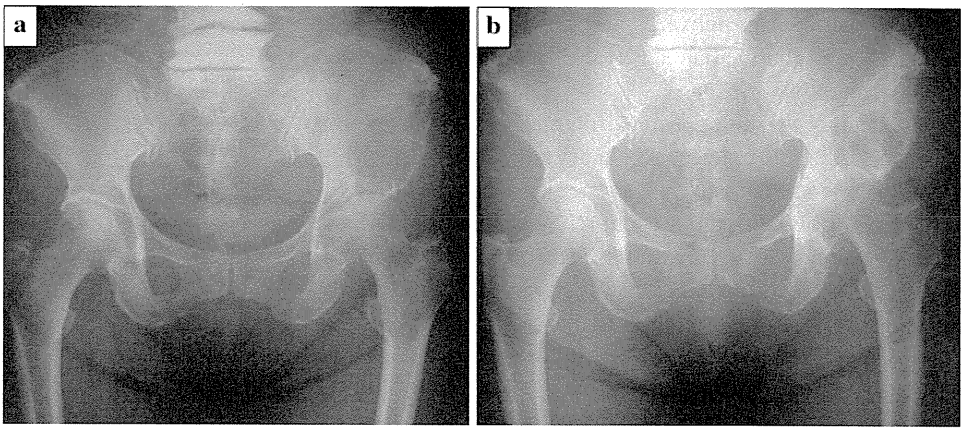

Fig. 4 Case 2. **a** Plain film shows the osteolytic lesion of bone metastases in the left ilium. **b** Plain film shows the prominent sclerotic change after local radiation therapy

If radiological imaging fails to confirm the location of the primary carcinoma site, biopsy is essential to rule out the possibility of the metastases being primary malignant bone tumors and to predict the cancer origin. In the present study, histopathological analysis revealed that the carcinoma types were adenocarcinoma in three cases, signet ring cell carcinoma in two cases and poorly differentiated carcinoma in two cases. Pavlidis et al. [3] reported that the histopathological types of carcinomas from primary unknown sites were mainly adenocarcinoma, followed by squamous cell carcinoma and poorly differentiated carcinoma. Prognosis of the patient differs depending on the type of carcinoma. Non-adenocarcinomas such as squamous cell carcinoma and neuroendocrine carcinoma have more favorable prognostic factors [1].

To investigate the location of the primary site of a carcinoma, FDG-PET imaging is being increasingly used. However, the efficacy of this approach is disputable. FDG-PET cannot be used to detect the presence of bone metastases, but can contribute in detecting extraskeletal metastases. Kole et al. [6] demonstrated that 27% of primary sites could be identified using FDG-PET after unsuccessful results using conventional diagnostic tools. In a review by Sève et al. [7] the detection rate of previously unknown primary tumor sites was found to be 41% using FDG-PET. We have been successful in using this modality for detecting primary carcinoma tumors at previously unknown sites.

At the first examination, multiple metastases, including bone and extraskeletal metastases, were already present in most cases. Systemic chemotherapy is the first choice of management for carcinoma metastases from unknown primary sites. Although systemic cancer chemotherapy should essentially be carried out according to conventional therapy protocols, an optimal standard chemotherapy regimen for carcinoma metastases from unknown primary sites has yet to be established. Multidrug regimens are generally administered as a first choice option. Previous reports [8–14] concerning representative systemic chemotherapy for carcinoma metastases from unknown primary sites, involving more than 50 patients, are summarized in Table 3.

Over the last two decades, the median survival time of patients with carcinoma metastases has been extended by approximately 7 months, due to the introduction of systemic chemotherapy using platinum. The administration of chemotherapy depends upon the general condition of the patient, but factors related to the therapeutic efficacy of chemotherapy may outweigh this consideration. More recently,

Table 3 Previous report on chemotherapy for carcinoma of unknown primary site

Authors	Year	No. of patients	Regimen	Response rate (%)	Survival median (months)	Reference
Bécouarn et al.	1989	85	5Fu/DOX/CDDP/HMM	21	7	[8]
Briasoulis et al.	1998	62	CBDCA/EPI/VP16	37.1	10	[9]
Greco et al.	2000	71	CBDCA/PTX/VP16	48	11	[10]
Briasoulis et al.	2000	77	CBDCA/PTX	38.7	13	[11]
Greco et al.	2002	120	CBDCA/PTX/GEM	25	9	[12]
Piga et al.	2004	102	CBDCA/DOX/VP16	26.5	9	[13]
Pittman et al.	2006	51	CBDCA/GEM	30.5	7.8	[14]

the administration of variable drug combinations, such as gemcitabine (GEM) and paclitaxel (TAX) in combination with platinum, has delivered improved response rates of 25–48%, and the median survival time has been increased to 9–11 months.

It appears that the patients diagnosed with carcinoma metastases from unknown primary sites have relatively limited life expectancy. The median survival time of patients involved in the present study was only 420 days. Hess et al. [1] reported that in their analysis of 1,000 patients, the median survival time was 11 months. Poor prognostic factors were age >61.5 years, the presence of liver metastases and tumor histologies other than neuroendocrine carcinoma and adrenal metastases [1]. In addition, the effect of bone metastases on survival depends on whether patients also have liver metastases. These factors may be important in the orthopedic oncologists' decision about whether or not to perform palliative surgery.

The limitation of the present study is that the number of patients was small and the power of the study is so limited, and the present study included the patients who were treated in a long span of 15 years, from March 1994 to 2009. In recent decades, early diagnosis using modern imaging techniques, such as whole body MRI and PET/CT, contribute to detect origin of primary sites in some cases [15]. And the extensive investigation with histopathological technology, immunohistochemistry [16, 17], electron microscopy [18] also gave some improvement for detection of primary site. Especially the therapeutic modality is also improving. Therefore, we may not evaluate the accurate up to date clinical features and result of the patients initially diagnosed with bone metastases from carcinoma with primary sites.

More recently, molecular gene profiling of carcinoma metastases biopsy samples has contributed to the detection of the primary site, and patients with metastases identified as originating from the colon have had a better response to their therapy [19]. It is now believed that in the future, such genetic analysis of biopsy samples will enable the delivery of cancer-specific treatments without the need for other costly and time-consuming diagnostic techniques.

Conflict of interest statement The authors declare that they have no conflict of interest.

References

1. Hess KR, Abbruzzese MC, Lenzi R, Raber MN, Abbruzzese JL (1999) Classification and regression tree analysis of 1,000 consecutive patients with unknown primary carcinoma. Clin Cancer Res 5:3403–3410
2. Rougraff BT (2003) Evaluation of the patient with carcinoma of unknown origin metastatic to bone. Clin Orthop Relat Res 415:105–109
3. Pavlidis N, Briasoulis E, Hainsworth J, Greco FA (2003) Diagnostic and therapeutic management of cancer of an unknown primary. Eur J Cancer 39:1990–2005
4. Katagiri H, Takahashi M, Inagaki J, Sugiura H, Ito S, Iwata H (2000) Determining the site of the primary cancer in patients with skeletal metastasis of unknown origin: a retrospective study. Cancer 88:1759–1761
5. Nottebaert M, Exner GU, von Hochstetter AR, Schreiber A (1989) Metastatic bone disease from occult carcinoma: a profile. Int Orthop 13:119–123
6. Kole AC, Nieweg OE, Pruim J, Hoekstra HJ, Koops HS, Roodenburg JL, Vaalburg W, Vermey A (1998) Detection of unknown occult primary tumors using positron emission tomography. Cancer 82:1160–1166
7. Sève P, Billotey C, Broussolle C, Dumontet C, Mackey JR (2007) The role of 2-deoxy-2-[F-18]fluoro-d-glucose positron emission tomography in disseminated carcinoma of unknown primary site. Cancer 109:292–299
8. Bécouarn Y, Brunet R, Barbé-Gaston C (1989) Fluorouracil, doxorubicin, cisplatin and altretamine in the treatment of metastatic carcinoma of unknown primary. Eur J Cancer Clin Oncol 25:861–865
9. Briasoulis E, Tsavaris N, Fountzilas G, Athanasiadis A, Kosmidis P, Bafaloukos D, Skarlos D, Samantas E, Pavlidis N (1998) Combination regimen with carboplatin, epirubicin and etoposide in metastatic carcinomas of unknown primary site: a Hellenic cooperative oncology group phase II study. Oncology 55:426–430
10. Greco FA, Burris HA 3rd, Erland JB, Gray JR, Kalman LA, Schreeder MT, Hainsworth JD (2000) Carcinoma of unknown primary site. Cancer 89:2655–2660
11. Briasoulis E, Kalofonos H, Bafaloukos D, Samantas E, Fountzilas G, Xiros N, Skarlos D, Christodoulou C, Kosmidis P, Pavlidis N